JBC RESEARCH ARTICLE

A novel strigolactone receptor antagonist provides insights into the structural inhibition, conditioning, and germination of the crop parasite *Striga*

Received for publication, November 30, 2021, and in revised form, February 12, 2022 Published, Papers in Press, February 16, 2022,
https://doi.org/10.1016/j.jbc.2022.101734

Amir Arellano-Saab[1,2], Christopher S. P. McErlean[3], Shelley Lumba[1], Alexei Savchenko[2,4], Peter J. Stogios[2,*], and Peter McCourt[1,*]

From the [1]Department of Cell and Systems Biology, and [2]Department of Chemical Engineering and Applied Chemistry, University of Toronto, Toronto, Ontario, Canada; [3]School of Chemistry, The University of Sydney, Camperdown, New South Wales, Australia; [4]Department of Microbiology, Immunology and Infectious Diseases, University of Calgary, Calgary, Alberta, Canada

Edited by Joseph Jez

Crop parasites of the *Striga* genera are a major biological deterrent to food security in Africa and are one of the largest obstacles to poverty alleviation on the continent. *Striga* seeds germinate by sensing small-molecule hormones, strigolactones (SLs), that emanate from host roots. Although SL receptors (*Striga hermonthica* HYPOSENSITIVE TO LIGHT [ShHTL]) have been identified, discerning their function has been difficult because these parasites cannot be easily grown under laboratory conditions. Moreover, many *Striga* species are obligate outcrossers that are not transformable, hence not amenable to genetic analysis. By combining phenotypic screening with ShHTL structural information and hybrid drug discovery methods, we discovered a potent SL perception inhibitor for *Striga*, dormirazine (DOZ). Structural analysis of this piperazine-based antagonist reveals a novel binding mechanism, distinct from that of known SLs, blocking access of the hormone to its receptor. Furthermore, DOZ reduces the flexibility of protein–protein interaction domains important for receptor signaling to downstream partners. *In planta*, we show, *via* temporal additions of DOZ, that SL receptors are required at a specific time during seed conditioning. This conditioning is essential to prime seed germination at the right time; thus, this SL-sensitive stage appears to be critical for adequate receptor signaling. Aside from uncovering a function for ShHTL during seed conditioning, these results suggest that future Ag-Biotech Solutions to *Striga* infestations will need to carefully time the application of antagonists to exploit receptor availability and outcompete natural SLs, critical elements for successful parasitic plant invasions.

Obligate plant parasites of the genus *Striga* infest a broad range of crops, including wheat, sorghum, maize, and millet, adversely affecting nearly 300 million people in sub-Saharan Africa (1, 2, 3). Aside from resulting in considerable economic loss, parasitic weeds are particularly devastating to subsistence farmers who often use agricultural practices that favor *Striga* infestations (1, 4, 5). The enormity of the *Striga* problem in Africa propels research into the genetics of crop host resistance and possible Ag-Chemicals Solutions to perturb the parasite (6, 7). The most pernicious parasitic species, *Striga hermonthica* (*Striga*), for example, dies within days of germination in the absence of a host. To circumvent this problem, *Striga* germinates only after seeds sense a small-molecule hormone, strigolactone (SL), exuded from newly planted crop roots (8). Breeding programs to reduce SLs in crops reduce parasitic seed germination in newly planted fields (9, 10). This approach, however, requires fine-tuning as crops also have hormonal needs for SL. Alternatively, SL agonists that stimulate *Striga* germination purge soil of viable parasitic seeds before crop planting (11, 12). Like most chemical solutions, this approach requires good chemical specificity, which in turn requires understanding the biology of the chemical targets.

Striga perceives SL through a collection of related α/β hydrolases designated *Striga hermonthica* HYPOSENSITIVE TO LIGHT (ShHTL), but the relationship of these small-molecule receptors to seed germination is complex (13). Seed responsiveness to SL requires specific temperatures and humidity, which in the field is achieved at the beginning of a new rainy season (14). Although this conditioning period (sometimes called preconditioning) is marked by complex receptor gene expression, the function of these patterns is unclear (15). Once seeds are conditioned, exposure to host SL results in a "wake-up phase" of receptor activity over the first 3 to 6 h at the embryo root tip followed by a longer "elongation tide" burst of activity after 15 h, mostly in the root meristematic region (15). Although *Striga* seeds do not physically germinate until the elongation tide, chemically perturbing the wake-up phase decreases germination (15). Because *Striga* is an obligate outcrossing species, connecting receptor function to seed conditioning and germination is experimentally challenging. Consequently, functions are mostly assigned by expressing *Striga* SL receptors in tractable genetic systems like *Arabidopsis thaliana* (*Arabidopsis*). Six receptors (ShHTL4–ShHTL9) impart SL sensitivity to *Arabidopsis* seeds, with ShHTL7 conferring SL hypersensitivity to levels observed for

* For correspondence: Peter J. Stogios, p.stogios@utoronto.ca; Peter McCourt, peter.mccourt@utoronto.ca.

Striga germination (16). These data, along with the observation that ShHTL7 activation is sufficient for *Striga* germination (16), indicate that this receptor is key to germination (11). Although SL agonists demonstrate the utility of chemical biology to probe *Striga* SL signaling function (11), the use of receptor antagonists, molecules that specifically bind to a protein and inactivate or impair it, for this purpose is lagging. Partly, this reflects the difficulty developing antagonist screens using *Striga* seed populations that are both genetically and physiologically variable. Phenotypic screens focused on nonparasitic plant SL receptors identify compounds that inhibit *Striga* germination, but unfortunately, in these model systems, SL interacts with a related DWARF14-type α/β hydrolase that has a different ligand-binding pocket (17). Notably, *Arabidopsis* encodes an ShHTL-like α/β hydrolase (HTL/KARRIKIN INSENSITIVE 2), but remarkably, this receptor does not bind naturally occurring (+)-(2′*R*) forms of SL but appears to bind non-natural (−)-(2′*S*)-SL enantiomers (Fig. S1*A*) (18). Thus, identification of *Striga*-specific antagonists using phenotypic screens has so far been unsuccessful.

An alternative to phenotypic screening is using the SL chemical scaffold to guide antagonist design, and such leads do block *Striga* seed germination (19, 20). Similar approaches have been used to find receptor hydrolase inhibitors, which also inhibit *Striga* germination (21). Both rational approaches, however, are limited with respect to the chemical space queried. And finally, although a more irrational approach of random library screening for receptor antagonists has not been done systematically, the serendipitous discovery that Triton X-100 binds ShHTL7 and moderately inhibits *Striga* germination indicates that compounds unrelated to SL chemistry can act as receptor antagonists (22).

With these issues in mind, we combined phenotypic-based germination screening with structural information on ShHTL7 to identify new SL-receptor antagonists specifically for analyzing *Striga* germination. We accomplished this by using a collection of SL antagonists first identified using *Arabidopsis* (23) and incubating them with purified ShHTL7; through X-ray crystallography, we found one, RG6, that forms a complex with this receptor. Structural information gleaned from this complex guided development of more antagonists for subsequent testing in phenotypic-based germination assays. Reiterating this process, performing structure similarity analyses and using molecular dynamics (MD) simulations led to the identification of a potent *Striga* germination inhibitor, dormirazine (DOZ). Temporal applications of DOZ strongly inhibited *Striga* seed germination when applied during seed conditioning indicating ShHTL receptors have functions before they sense host-derived SL. Intriguingly, similar experiments using an *Arabidopsis* line expressing ShHTL7 found that SL receptors can also signal during seed conditioning, tuning seed responses to future germination cues. These results suggest that, although *Striga* seeds uniquely tether their germination response to SL, they share seed conditioning mechanisms with nonparasitic plants that ensure seeds will not germinate too early or too late in their respective environments. Importantly, these results also suggest that development of SL antagonists for *Striga* management strategies should take into account time of application during parasitic plant infestations.

Results

Structural characterization of the ShHTL7–RG6 complex

Using an SL-dependent hypocotyl-shortening assay, we previously identified seven compounds (RG1–RG7) that appear to act as SL antagonists on *Arabidopsis* (Fig. S1*B*) (23). Because one compound, dubbed soporidine, binds ShHTL7 receptors, we tested to see if any other RG compounds could complex with ShHTL7 protein in a crystallization assay and obtained a structure of RG6 bound to the ShHTL7-binding pocket to a resolution of 1.46 Å (Fig. 1*A*). ShHTL7, like all characterized SL receptors, forms a catalytic triad of serine (Ser95), histidine (His246), and aspartate (Asp217) amino acids that hydrolyze bound SL (24). Interestingly, the methoxyphenyl group of RG6 is positioned relatively far from Asp217 and His246 (4.2 and 7.9 Å, respectively) and slightly closer to the catalytic nucleophile Ser95 (3.6 Å). Notably, most of the RG6–ShHTL7 contacts are located on the interior side of the upper left lid domain of the protein (Fig. 1*B*). In total, 12 hydrophobic interactions and one H-bond (2.8 Å) were observed within the complex (Fig. 1*C*). We also noted strong electron density that modeled as a glycerol molecule interacting with two residues, Phe134 and Thr157, which are located on the right lid domain, and with Ile218, a neighboring residue to the catalytic Asp217 (Fig. 1*D*). The positioning of this glycerol molecule is important given that the sites where it makes contact could be further exploited for rational antagonist design.

The positioning RG6 with ShHTL7 indicates that it likely antagonizes SL by obstructing accessibility to the binding pocket. We tested this by docking the synthetic SL, (+)-(2′*R*)-(GR24), into the active site of ShHTL7 using an alignment based on a DWARF14-type receptor structure associated with a hydrolyzed GR24 intermediate (25) and compared it with our RG6–ShHTL7 structure. The orientations of (+)-(2′*R*)-GR24 and RG6 were opposite when the binding pocket is viewed frontally, with (+)-(2′*R*)-GR24 positioned at an angle of ∼105°, whereas RG6 was located at an angle of ∼80° relative to Ser95 (Fig. 1*E*). Moreover, unlike RG6, the D-ring of (+)-(2′*R*)-GR24 interacts with Ser95 and His246 of the catalytic triad. This analysis indicates that SL positioning within a receptor should not be the only reference for rational designing of ligands, a conclusion consistent with the modeling of the SL agonist sphynolactone-7 (SPL7) (11). In addition, we confirmed the specificity of RG6 toward sensitive SL receptors by docking it into ShHTL5, another highly sensitive receptor, and ShHTL3, a receptor that is thought not to bind SLs (26). This analysis revealed that RG6 would generate a medium-strength interaction with ShHTL5 because of its medium-sized pocket. RG6, however, does not fit well in the more constricted ShHTL3 pocket, and several clashes would be generated, resulting in an unlikely interaction (Fig. S2). Finally, the RG6–ShHTL7

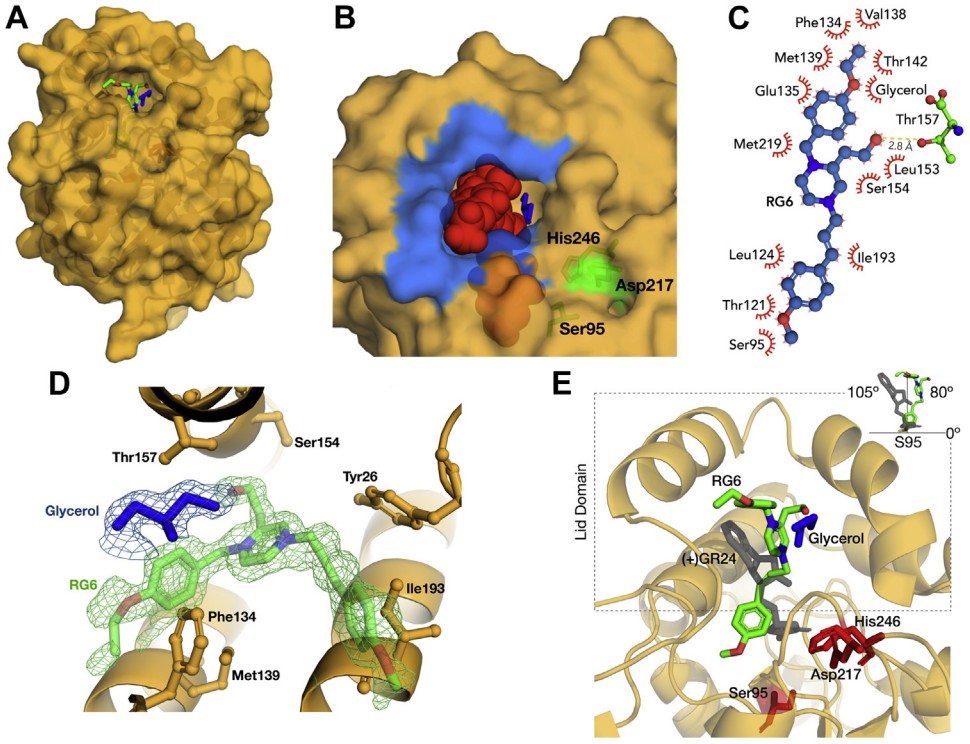

Figure 1. RG6 specifically inhibits ShHTL7. *A*, crystallographic structure of ShHTL7 complexed with RG6 (*green sticks*) and glycerol (*dark blue sticks*) (PDB ID: 7SNU). *B*, RG6 (*red spheres*) blocks the entry to the active site of ShHTL7, preventing the access of an SL molecule. Protein contacts are indicated in *light blue*, and catalytic triad residues are indicated in *green*. *C*, detailed interactions between RG6 and ShHTL7 residues. *Red fans* indicate hydrophobic contacts, hydrogen bond is indicated by the *yellow dotted line*. *D*, electron density maps for RG6 (*green*) and glycerol (*blue*) occupancy (horizontal rotation to facilitate viewing). Closely interacting ShHTL7 residues are shown with *sticks*; panel shows simulated annealing, F_c–F_o maps, isosurface mesh rendered at 1 Å. *E*, the binding mechanisms of RG6 and (+)-(2*R*′)-GR24 to ShHTL7. RG6 is positioned 80° in reference to Ser95, whereas (+)-(2*R*′)-GR24 (*gray sticks*) is found close to the catalytic triad residues (*red sticks*) at an angle of 105° in reference to Ser95, as shown in the *upper right corner* of the panel. Lid domain is outlined with a *dotted line*. PDB, Protein Data Bank; ShHTL7, *Striga hermonthica* HYPOSENSITIVE TO LIGHT; SL, strigolactone.

complex did not result in significant structural changes within the receptor compared with apoprotein structures, suggesting RG6 locks ShHTL7 into an inactive open state (27). Recent studies suggest that flexibility in the lid region, particularly in the αE loop of α/β hydrolase receptors, is key for SL binding and attracting downstream signaling partners (28, 29, 30). Possibly, RG6 reduces this flexibility, which would contribute to the inhibition of downstream signaling.

RG6 chemical optimization

With RG6–ShHTL7 structural information, we next used a drug design computational approach to optimize ligand binding. First, we screened the CORE and EXPRESS-Pick Library stocks (ChemBridge), commercially available small-molecule libraries, for nonhydrolyzable compounds with similar structures to RG6 (2D and 3D Tanimoto similarity ≥85%) and identified 21 lead compounds. Compounds were docked using AutoDock (31), a program that considers protein flexibility, and SwissDock (32), which ranks ligand–protein interactions based on binding modes; in addition, we looked for compounds that could fully obstruct the entry to the binding pocket based on the glycerol–ShHTL7 interactions. Seven compounds did not dock properly and were removed from further analysis leaving us with 14 RG6-series compounds (RG6-1 to RG6-14) (Table S1*A*). From this list, two compounds, RG6-4 and RG6-6, stood out as having low ΔG values and relatively high full fitness value binding likelihoods into the active site of ShHTL7 (Table S1*B*). To characterize our RG6 series further, we phenotypically screened all 14 compounds against *Arabidopsis* lines, each expressing a high-affinity *Striga* SL receptor (ShHTL4–ShHTL9). Normally, ShHTL-expressing seeds germinate poorly at high temperatures, but this thermoinhibition is overcome by the addition of SL (33). All 14 leads reduced the ability of *rac*-GR24 (a racemic mixture of (+)-(2′*R*) and (-)-(2′*S*) isomers) to germinate thermoinhibited seed, suggesting this series of leads inhibit all these receptors to some degree (Fig. 2*A*). Interestingly, although *in silico* analysis suggests RG6-4 and RG6-6 have similar affinities for ShHTL7, RG6-6 was a better SL inhibitor across all transgenic lines tested, with strong efficacy on ShHTL7-expressing lines (Fig. 2*A*).

Based on the potency of RG6-6 in our SL germination assays, we rescreened the ChemBridge libraries using this structure and identified 21 compounds with similarity to RG6-6 (3D Tanimoto similarity ≥85%). Repeating our docking analysis enriched for 18 lead compounds designated the RG6-6 series (Table S2). We refined this list *via* MD simulations, an atomic-level technique that explores the dynamic energy landscapes of ligand-docked proteins. Using triplicate 0.5 μs simulations, we calculated free-energy scores and average potential energies categorizing our MD simulations into three

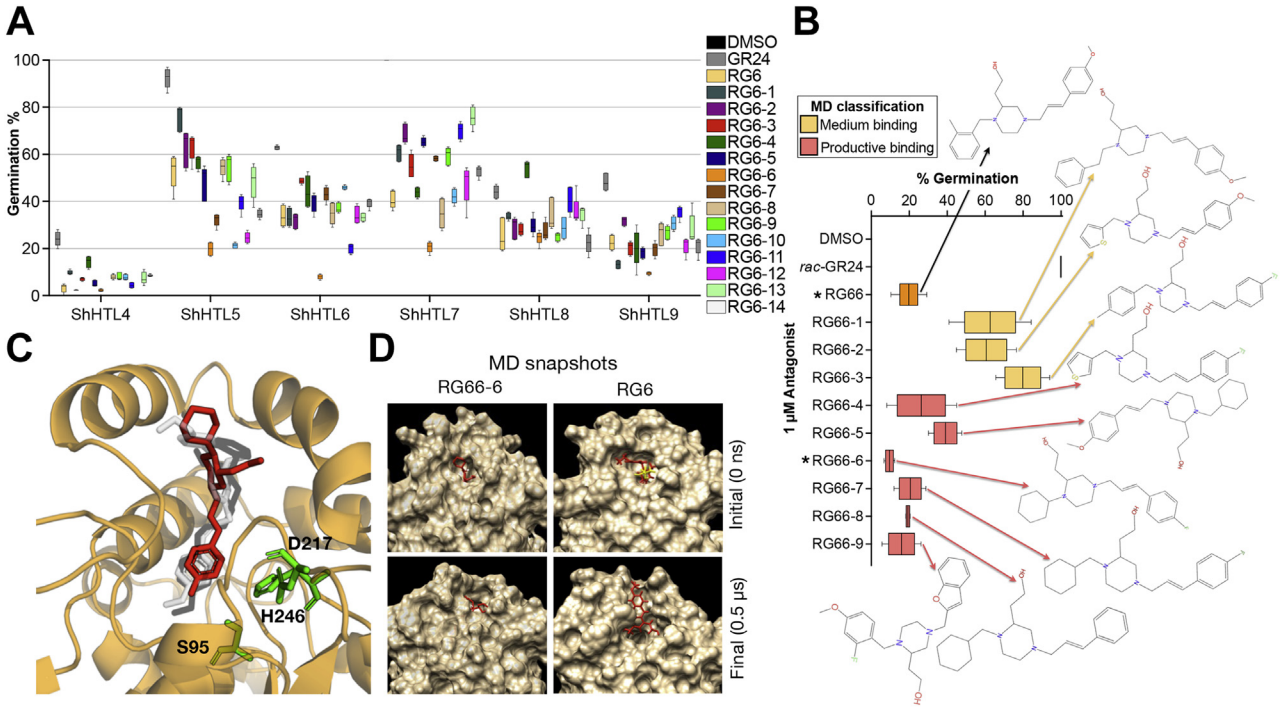

Figure 2. Hybrid optimization of RG6-related compounds. *A*, germination of thermoinhibited transgenic *Arabidopsis* lines, each expressing a collection of SL-sensitive ShHTL receptors in the presence of the strigolactone, *rac*-GR24 (1 μM), and 1 μM of candidate molecule. No thermoinhibited lines germinated on the DMSO-only control. Each box represents three sets of biological replicates of >50 seeds each; interior bars represent mean; error bars represent SD. *B*, structures of RG66-series lead compounds as assessed by inhibition of germination using an *Arabidopsis* GA-depletion assay. GA-depleted *Arabidopsis* lines germinate to 100% (*gray*) in the presence of 1 μM *rac*-GR24. Each box represents three sets of biological replicates of >50 seeds each; interior bars represent mean; error bars represent SD. $*p < 0.05$ relative to control treatment using a two-tailed Student's *t* test. *C*, superposition of RG6 (*gray*), RG6-6 (*black*), and RG66-6 (*red*) on the active site of ShHTL7 to visualize differences in their binding modes. *D*, initial and final snapshots of the MD simulations for RG6 and RG66-6 complexed (*red sticks*) with ShHTL7 show the overall movement reduction and chemical binding positions through the simulation. DMSO, dimethyl sulfoxide; GA, gibberellin; MD, molecular dynamics; ShHTL, *Striga hermonthica* HYPOSENSITIVE TO LIGHT; SL, strigolactone.

groups: (1) productive binders that interacted with residues Tyr26, Ser95, Phe134, Ile193, and Met219 for >80% of the simulation time; (2) intermediate binders that interacted with at least three of the five residues for 80% of the simulation time; and (3) unlikely binders that either had only two interactions in total or more than two interactions <50% of the simulation time. The visual MD and RMSD modules of GROMACS (GROningen MAchine for Chemical Simulations) also indicated that less effective binders had higher RMSD values, longer convergence time points, and greater average potential energies resulting from a tendency to dissociate from the active site of the protein (Table S2). When we extracted individual snapshots of a simulation to compare the compounds' behavior at different stages of the simulation, productive binders remained within the binding pocket throughout the simulation. By contrast, weaker binders dissociated after roughly 0.3 μs (Fig. S3). Informed by these results and using our categorizing cutoffs, we classified nine compounds as either highly or moderately effective (Table S2 and Fig. S4).

We next phenotypically screened these nine RG6-6-series compounds against an ShHTL7-expressing *Arabidopsis* line using a recently developed SL-dependent germination assay involving depletion of the germination stimulant hormone gibberellin (GA) (34). Overall, the levels of SL antagonism agreed with our *in silico* analyses; compounds predicted as effective binders were the most potent SL antagonists with RG66-6 reducing *rac*-GR24–induced germination to approximately 13% (Fig. 2*B*). Docking analyses to ShHTL7 indicated that, like RG6, the piperazine moiety of RG66-6 is found in the space created by the lid domain, whereas its cyclohexyl group is blocking entry to the active site (Figs. 2*C* and S5). In contrast to RG6 and RG6-6, which have methoxy benzene rings that interact with the active site of ShHTL7, RG66-6 has a substituted fluoride atom (Figs. 2*C* and S4). This fluoride atom of RG66-6 interacts with Leu124 and the two catalytic triad amino acids Ser95 and His246. On the other side of the compound, the moiety predicted to interact mainly with the lid domain seems to be the most variable element; with RG6 having an ethoxy benzene group, RG6-6 having a simpler methylbenzene/toluene group and RG66-6 exhibiting a fairly simple cyclohexyl substitution (Fig. S4). This analysis suggests that molecules with piperazine moieties coupled to flexible backbones, possibly containing fluoride or similar atoms, are most favorable for binding to ShHTL7.

Consistent with the *in planta* germination inhibition, trajectories of 0.5 μs MD simulations for RG66-6 and RG6 showed that both molecules consistently remained in the binding pocket of ShHTL7. However, RG66-6 was more effective at stabilizing and reducing the motility of the αE loop, an effect attributed to tighter binding (Fig. 2*D* and Movie S1). The motion of the αE loop and the upper left lid

domain are thought to be important in SL signaling (28, 29, 35). Our previous MD simulation findings for a chimeric SL receptor and GR24 indicate that, upon binding to an SL, the αE loop of the protein increases its motion, to facilitate a conformational change and achieve signaling (28). This analysis reiterates the notion that reducing flexibility of the αE loop should be considered a desirable feature of potent SL antagonists.

Biochemical characterization of RG66-6

To biochemically characterize RG66-6, we first used differential scanning fluorimetry (DSF), which monitors receptor–ligand interactions by protein melting temperature (T_m) shifts. As expected, binding of *rac*-GR24 to ShHTL7 decreased its T_m by approximately 2.5 °C *versus* the mock-treated receptor (Figs. 3*A* and S6). This T_m decrease, however, was suppressed in the presence of RG66-6, consistent with this compound inhibiting the SL access to the ShHTL7-binding pocket (Fig. 3*A*). Next, we tested the ability of RG66-6 to inhibit ShHTL7 hydrolysis activity using Yoshimulactone Green (YLG), a probe that releases fluorescein when hydrolyzed by this receptor (15). Hence, progressive inhibition of YLG-dependent fluorescence by competition with SL is an indirect measure of the potency of a compound to bind ShHTL7. Among the three inhibitors (RG6, RG6-6, and RG66-6), RG66-6 was the most potent SL competitor (IC_{50} = 0.28 μM) compared with either RG6 (IC_{50} = 1.54 μM) or RG6-6 (IC_{50} = 0.67 μM) (Fig. 3*B*). Interestingly, although RG66-6 is an order of magnitude more potent at inhibiting *Striga* germination *versus* Triton X-100, the reported ShHTL7 YLG IC_{50} value for this detergent is in the nanomolar range (22). This discrepancy most likely reflects the long preincubation treatment of ShHTL7 in Triton X-100, which was not carried out in this study (15). By removing this preincubation step, we determined an IC_{50} of 4.72 μM for this compound, more than 16 times higher than that of RG66-6 (Fig. S7).

To compare the potency of the three antagonists using a direct method, we titrated increasing amounts of each in the presence of ShHTL7 and determined their T_m using DSF. Then, we used the DSF-fitting algorithm (36) to calculate the dissociation constant (K_d) for each compound. RG6 showed the highest K_d of 4.54 μM, followed by RG6-6 of 1.27 μM and RG66-6 of 0.26 μM (Fig. S8). Overall, these dissociation constants agree with the predictions generated by our *in silico* experiments; particularly in this case, we observed a correlation between the potency of the compounds and their Gibbs free energies (Table S2).

Based on the high inhibitory potency shown by the antagonists in our biochemical experiments, we tested them directly on *Striga* seeds. RG66-6 was the best inhibitor of *rac*-GR24–induced *Striga* seeds germination with an *in vivo* germination IC_{50} of 1.82 μM followed by RG6-6 (IC_{50} = 2.52 μM) and RG6 (IC_{50} = 6.85 μM) (Fig. 3*C*). Although the order of magnitude of these compounds between biochemical and functional studies is maintained, there is a small difference in the potency of inhibition. This divergence may reflect either the stability and hydrolytic properties of ShHTL7 *in vitro*, which may be suboptimal because of the absence of downstream signaling partners, or the lack of cellular cofactors, such as MAX2 or SMAX1 (37, 38, 39), or the slightly decreased ability of the compounds to penetrate the seed coat. Whatever the case, because RG66-6 inhibited *Striga* seed germination at low micromolar concentrations, we renamed the compound DOZ from the Latin word *dormire*, meaning to sleep, and for the piperazine moiety in its chemical structure.

Striga *SL responsiveness requires receptor activation during seed conditioning*

Although ShHTL receptors show complex patterns of activity during seed development, it is unclear how these patterns translate to the germination response (15). To test the role of

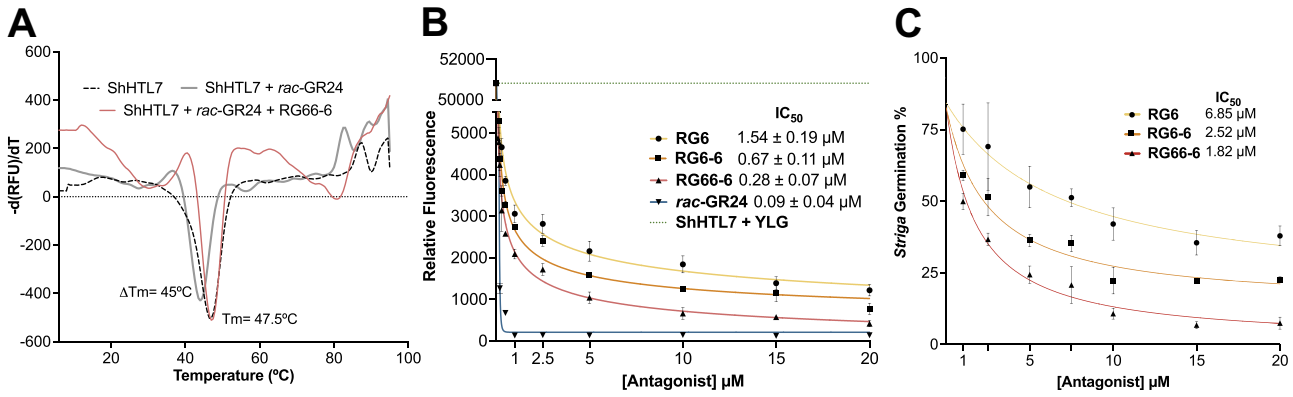

Figure 3. Biochemical characterization of RG66-6. *A*, DSF melting temperature curves of ShHTL7 protein preincubated with 1 μM *rac*-GR24 in the absence or the presence of 2.5 μM RG66-6. A derivative of the change in fluorescence because of gradual protein unfolding was plotted against temperature. These curves were used to calculate inflection points of fluorescence *versus* temperature (T_m). Each *line* represents the average protein melt curve for three replicate samples. *B*, YLG hydrolysis inhibition using purified ShHTL7 over increasing concentrations of RG6, RG6-6, RG66-6, and *rac*-GR24. The progressive addition of higher concentrations of the antagonists reduces the hydrolysis ability of ShHTL7, resulting in a lower relative fluorescence, following a similar inhibition pattern to that displayed by *rac*-GR24. Error bars represent SD across three independent replicates. IC_{50} values were calculated from three independent replicates. *C*, germination inhibition of *Striga* seeds on increasing concentrations of antagonists. All treatments were in the presence of 1 μM *rac*-GR24. Average half-maximal inhibitory concentrations (IC_{50}) were calculated from three biological replicates of >50 seeds each; error bars represent SD. DSF, differential scanning fluorimetry; ShHTL7, *Striga hermonthica* HYPOSENSITIVE TO LIGHT; YLG, Yoshimulactone Green.

ShHTL receptors through *Striga* seed development, we temporally applied 1 μM DOZ to seeds at different stages of development and measured its impact on *Striga* germination. Addition of DOZ only during *Striga* seed conditioning noticeably reduced the ability of SL to induce germination, suggesting ShHTL receptors have an essential function during this stage in the establishment of seed responsiveness to future exposures of host-derived SL (Fig. 4*A*). By contrast, addition of DOZ at various times up to 24 h after *Striga* seed conditioning resulted in a more discrete effect, with 1 μM DOZ inhibiting ∼50% of *Striga* germination after 24 h of exposure (Fig. 4*B*). These results are a clear precedent that time of antagonist application and the environmental conditions for this application should be considered when dealing with in-field *Striga* infestations. Furthermore, our results indicate that exposure to the antagonist before SL conditioning could increase their potency, possibly because of the reduced competition for the SL receptor's binding site.

To further probe the function of ShHTL receptors during seed conditioning, we took advantage of the ability of SL to bypass the germination requirement of GA in an *Arabidopsis* line expressing ShHTL7 (34). Seeds of *Arabidopsis*, like many nonparasitic plants, use cold conditioning to increase their levels of responsiveness to dormancy-breaking stimulants, like GA, and it has been posited that *Striga* seed conditioning may be analogous to breaking primary seed dormancy (40). Expressing ShHTLs in *Arabidopsis* seeds makes inhibition of downstream HTL/KARRIKIN INSENSITIVE 2 germination repressors dependent on SL addition; however, like *Striga*, we are not sure when this happens (34). Application of DOZ to ShHTL7-expressing *Arabidopsis* during cold conditioning blocked the ability of *rac*-GR24 to circumvent the requirement of GA for germination (Fig. 4*C*). This suggests that cold conditioning of *Arabidopsis* seeds has mechanistic parallels with *Striga* seed conditioning, and SL receptors can impinge on these processes.

Discussion

Screening for active small molecules usually involves scoring a specific cellular or whole organism phenotype, or if the target is known and well characterized, developing a biochemical-based approach (41). Phenotypic screening has the advantage that compounds can be queried in complex environments to reflect a more physiological situation, but these screens must be simple, cheap, and reproducible (42). In addition, connecting leads to specific targets can be challenging. Targeted approaches, by definition, are focused, but they are also limited to available biochemical or structural information. In this study, we used a hybrid approach cycling between phenotypic screening using seed germination and target-based structural information to identify a new antagonist of SL perception, DOZ in the noxious weed *Striga*. The increased potency of DOZ most likely reflects our ability to focus on a key SL receptor in *Striga* germination, ShHTL7, *versus* other chemical approaches that center first on nonparasitic SL receptors before testing on *Striga* (43). Even with this ShHTL7 focus, however, DOZ appears to inhibit multiple receptors to varying degrees, a possible result of the innate promiscuity of SL receptors (28, 44).

Properties of efficient Striga *SL antagonists*

The identification of RG6 complexed with ShHTL7 is a useful foundation for guiding the development of new SL receptor antagonists. Comparison of the binding mode of the experimentally determined RG6 with modeling of RG6-6, DOZ, and (+)-(2′*R*)-GR24 allows comparisons between the compound potency and the number of interactions with the ShHTL7 protein (Fig. 5). Recently, three amino acids (Leu153, Thr157, and Thr190) have been shown to be functionally important for SL recognition (28). All three antagonists interact with Leu153 and Thr157, but the least effective antagonist, RG6, does not interact with Thr190 (Fig. 5). If we

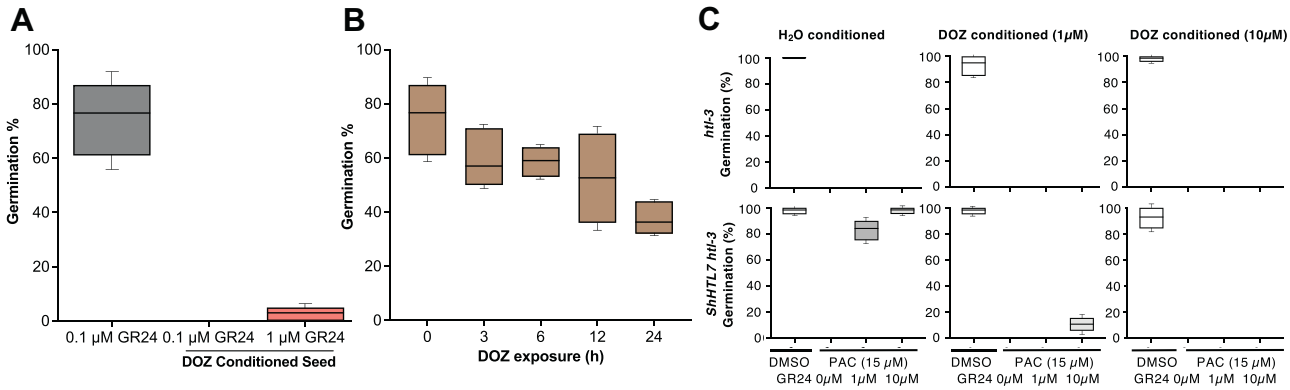

Figure 4. Dormirazine (DOZ) perturbs seed conditioning in both *Striga* and *Arabidopsis*. *A*, germination of *Striga* seeds conditioned on *rac*-GR24 in the presence of 1 μM DOZ. Each box represents three sets of biological replicates of >50 seeds each; interior bars represent mean; error bars represent SD. *B*, germination of *Striga* seeds on 0.1 μM *rac*-GR24 after conditioning in the presence of increasing exposure times to 1 μM DOZ. Each box represents three sets of biological replicates of >50 seeds each; interior bars represent mean; error bars represent SD. *C*, DOZ blocks SL-induced germination during cold conditioning of ShHTL7-expressing *Arabidopsis*. Control treatment represents minimal media with DMSO; all other treatments were performed in the presence of 15 μM paclobutrazol (PAC) and increasing concentrations of *rac*-GR24. *Arabidopsis* lines with a depleted HTL receptor (*htl-3*) were used as negative controls. Each box represents three sets of biological replicates of >50 seeds each; interior bars represent mean; error bars represent SD. DMSO, dimethyl sulfoxide; ShHTL7, *Striga hermonthica* HYPOSENSITIVE TO LIGHT; SL, strigolactone.

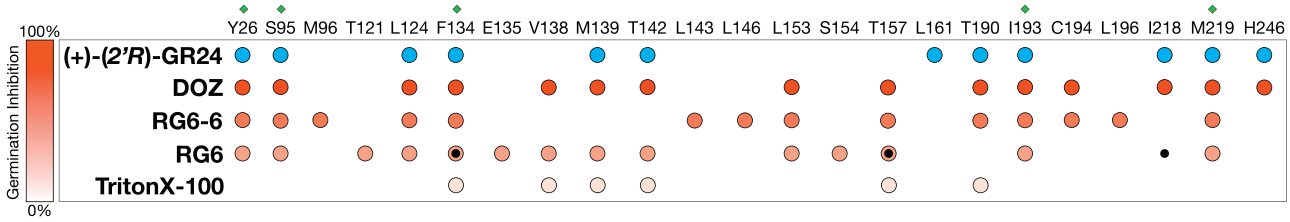

Figure 5. Rationalization of effective SL antagonists. Map of interactions between ShHTL7 amino acid residues with (+)-(2*R*′)-GR24 (*blue circles*) and four antagonists (*red circles*). Antagonists are arranged based on their germination inhibition potency (gradient scale). *Green diamonds* at the *top* indicate selected reference residues for the analysis of MD binding modes. *Black circles* indicate interactions between glycerol and ShHTL7 in the RG6 structure. MD, molecular dynamics; ShHTL7, *Striga hermonthica* HYPOSENSITIVE TO LIGHT; SL, strigolactone.

broaden our analysis, RG6 shows 14 contact points with ShHTL7, eight of them coinciding with one of the 12 amino acids that contact (+)-(2′*R*)-GR24 (Fig. 5). By contrast, RG6-6 and DOZ have 15 potential interactions with ShHTL7, with the less potent RG6-6 sharing seven (+)-(2′*R*)-GR24 contact points and DOZ sharing 11 contacts (Fig. 5).

Our structural studies also revealed that RG6-derived compounds interact with the ShHTL7 lid domain amino acids that would not contact (+)-(2′*R*)-GR24 (Fig. 5). Recent studies show that increasing overall elasticity of SL receptors, which involves lid amino acids, is thought to be important for interactions with downstream signaling partners; consistent with this, RG6 complexed with ShHTL7 appears to lock the receptor into an open nonactive conformation (28, 29, 35, 30). On this note, the binding of the detergent Triton X-100 to the lid of ShHTL7 and its ability to moderately inhibit *Striga* germination also supports targeting lid domain amino acids in the development of new SL receptor antagonists (22). Our analysis of Triton X-100, however, identified only six potential interactions with ShHTL7, of which merely three overlap with (+)-(2′*R*)-GR24 contact points (Fig. 5). Aside from issues of specificity of this detergent, this low level of interaction most likely explains why it is a relatively poor antagonist of *Striga* germination.

Finally, in this study, we gleaned information on protein flexibility and protein–ligand interactions using MD simulations, which correlated well with the biological activity experimentally observed. In addition, these technologies helped discern binding differences between compounds and probe how crystallization artifacts can locate transiently within the binding pocket. Nevertheless, although the glycerol molecule in our ShHTL7 structure is a transient artifact, our structural screening exploited its position to search for compounds with potential to contact the same residues (Fig. 5); these additional contacts might have contributed to the increased inhibition ability of RG6-6 and DOZ and should be considered when designing future antagonists. Interestingly, using MD and small-molecule docking, we observed that the binding modes of RG6, RG6-6, and DOZ appear to be very similar (Fig. 2*C*); however, subtle differences in the number and position of the amino acids they contact appear to be key in their inhibitory potency. In addition, these compounds target most of the residues that SL molecules and agonists such as SPL7 bind to (Figs. 5 and S9), indicating that targeting these positions is key in preventing SL-induced signaling. In summary, this signaling is thought to be blocked through a mechanism derived from three actions: (a) physically blocking entry to the binding pocket, (b) binding to at least the same residues SLs need to exert their action, and (c) prevent SL hydrolysis, impeding a conformational change that leads to signaling and germination.

Although many of the *in silico* tools used in this study are common to pharma-based studies (45, 46), they are not extensively used in Ag-Biotech compound discovery. We believe as more plant protein structures are discerned, particularly with the advent of programs, such as AlphaFold (47) and RoseTTAFold (48), this information combined with dynamics simulations will greatly improve drug discovery for agricultural purposes.

A role for SL receptors in seed conditioning

Seed dormancy is an acquired trait that allows seeds to determine when environments are favorable for germination cues (40). Although in *Striga*, host-derived SL is a germination cue, it is not the only essential component (14). Seed conditioning usually involves specific durations of temperature and humidity, and in *Striga*, either insufficient or excessive conditioning reduces SL responsiveness. It is thought that these precise requirements ensure *Striga* seeds germinate at appropriate times to maximize host infections; consistently, delayed planting of crops, for example, affects *Striga* germination efficiency and therefore infestations (49, 50).

Although the strict dependency of *Striga* germination on SL is unique, *Striga* seed conditioning has parallels to cold seed stratification of winter annual plants like *Arabidopsis* (40). In this scenario, *Striga* seed conditioning is analogous to breaking primary dormancy and allowing seeds to become responsive to germination stimulants, whereas prolonged conditioning is akin to re-establishing secondary dormancy and reducing seed responsiveness to stimulants. It is thought that primary and secondary dormancy make sure seeds do not germinate too soon or too late in the season despite the presence of optimal environmental conditions (40). We also found *Arabidopsis* expressing the *Striga* SL receptor, ShHTL7, influenced seed conditioning. SL in *Striga* and an unidentified butenolide (KL) in *Arabidopsis* both regulate the same downstream effectors to control germination so perhaps similarities between parasitic and nonparasitic seed germination are not astonishing (34). It is, however,

surprising that conditioning seeds for future responsiveness to SL uses SL signaling pathways. In *Striga*, for example, the source of SL that activates receptors during seed condition in the absence of a host is unclear, and why these activated receptors do not germinate *Striga* seeds during conditioning is confounding. Possibly, *Striga* seeds synthesize just enough SL to condition its own seeds but not enough for germination; nevertheless, this seem unlikely, as conditioned seeds are exquisitely sensitive to SL (51). Alternatively, binding of DOZ to SL receptors might inhibit SL-independent functions. DOZ most certainly changes ShHTL receptor elasticity, and perhaps this change in flexibility in the absence of SL is important for uncharacterized ShHTL functions during seed conditioning.

By contrast, inhibiting ShHTL activation by SL after seed conditioning did not dramatically reduce germination. This observation is at odds with receptor agonist experiments that indicate that the wake-up phase of receptor activation is important for germination (15). One difference between receptor agonist *versus* antagonist experiments is an agonist may only need to activate one or a small portion of receptor to activate germination. To this point, SPL7, which only activates ShHTL7, is sufficient to stimulant *Striga* germination (11). By contrast, an antagonist most likely will need to inhibit all expressed receptors to have a phenotypic effect and therefore may not be as potent as an agonist. It is also possible the lack of a strong DOZ inhibitory response after seed conditioning reflects poor compound accessibility to ShHTL receptors at this stage of development. This does not seem plausible as DOZ works well during seed conditioning. Finally, expression of ShHTL4 through ShHTL7 genes does increase during seed conditioning, which may mean more antagonists are required to inhibit more target receptors (15). Whatever the case, the sensitivity of the *Striga* seed germination to DOZ inhibition during conditioning indicates this phase of development is very sensitive to chemical perturbation. This information will be useful in designing screens for the development of new SL perception antagonists and provides further insight into when and how to apply SL antagonists as herbicides to combat *Striga*-infested fields.

Experimental procedures

Protein expression and purification

Protein coding sequence for ShHTL7 (codon optimized) was cloned into pMCSG53 and p15-TEV-LIC and transformed into BL21-Gold (DE3) *Escherichia coli* cells, which were subsequently grown at 37 °C on LB media until an absorbance of 0.6 to 0.8 at 600 nm. Protein expression was then induced using 1 mM IPTG shaking at 200 rpm overnight at 17 °C. Cells were harvested and resuspended in a buffer containing 0.3 M NaCl, 50 mM Hepes (pH 7.5), 5 mM imidazole, and 5% glycerol. ShHTL7 protein was purified and eluted using His nickel-affinity chromatography, washing with increasing concentrations of imidazole (30–250 mM). The 6×-histidine tag was cleaved by adding 60 μg of tobacco etch virus protease per 1 mg of protein and dialyzed overnight at 4 °C in a buffer containing 0.3 M NaCl, 50 mM Hepes (pH 7.5), and 5% glycerol. Tag removal and preliminary purity were checked by SDS-PAGE. Finally, the protein was purified by FPLC against a final elution buffer consisting of 0.15 M NaCl, 10 mM Hepes (pH 7.5), and 1 mM Tris(2-carboxyethyl)phosphine. Fresh protein preparations were used for crystallization and subsequent biochemical assays.

Crystallization, X-ray diffraction data collection, and structural analysis

ShHTL7 was screened for crystallization using a Mosquito LCP crystallization robot (TTP Labtech) in sitting drop 96-well format using a custom in-house suite of crystallization conditions (52) and in the presence of 0.1 mM RG1–RG7. ShHTL7 crystallized in the presence of RG6, and diffraction quality crystals were grown at room temperature using the hanging drop method, with 1.5 μl of 8.5 mg/ml protein solution mixed with 1.5 μl of reservoir solution (1 M sodium acetate, 0.1 M imidazole [pH 7.0], and 5% glycerol). The crystal was cryoprotected with paratone oil before X-ray diffraction screening. Screening diffraction images at 100 K were collected on a Rigaku Micromax-007 HF rotating copper anode source with a Rigaku RAXIS-HTC. Final diffraction data for the ShHTL7–RG6 complex were collected at 100 K at the Life Sciences Collaborative Access Team beamline 21-ID-D at the Advanced Photon Source, Argonne National Laboratory. X-ray data were reduced with HKL-3000 (53). The structure of ShHTL7–RG6 was solved by molecular replacement using the structure of ShHTL5 (Protein Data Bank [PDB] ID: 5CBK) as a search model in Phenix.phaser (Phenix) (54). Manual model adjustment was performed with Coot (55). *B*-factors were refined as isotropic, and translation/libration/screw parameterization was included. The final ShHTL7 model includes residues 3 to 270 of the protein. Geometry was verified using the Phenix and Coot validation tools plus the wwPDB deposition server. X-ray crystallography statistics are shown in Table S3. The structure factors and atomic coordinates for the ShHTL7–RG6 structure were validated and deposited into the PDB (PDB ID: 7SNU). Protein structural analysis and figures were produced with PyMOL, version 2.1 (Schrödinger) (56). Protein–ligand interactions were calculated with LigPlot+ (57).

Chemical docking

The docking of all candidate chemicals (from the CORE and EXPRESS-Pick Library stocks) into the structure of ShHTL7 was performed using SwissDock (32) and AutoDock (31). Flexible residues were manually selected on AutoDock from the lid domain (Lys137–Leu155) and the flexibility loop (Cys164–Ser168). The top binding pose for each compound was selected based on the lowest Gibbs free energy (Tables S1*B* and S2); a cutoff Gibbs free energy value of −1 kcal mol^{-1} (AutoDock) and −1000 full fitness score units (SwissDock) was set for initial evaluation and discrimination. Prospective compounds with a likely interaction energy score were then inspected using the University of California, San Francisco Chimera viewer to verify that no clashes with the

protein would be generated. Minimal differences were observed between the most energetically favored binding states obtained by the two docking engines, so further analysis for the MD pipeline and productivity classification was carried out with the SwissDock models, as these reflected the lowest free energy values on average.

Thermoinhibition screening

One- to 2-month-old Col-0 *Arabidopsis* seeds with *htl-3* background expressing ShHTL4–ShHTL9 (16) were surface sterilized with 70–100% (v/v) EtOH and dried with a speed vacuum. Germination assays were performed on 48-well plates containing 200 µl of 1/2 Murashige and Skoog (MS) minimal agar medium, and several concentrations (0–100 µM) of candidate molecule dissolved in dimethyl sulfoxide, in the presence of 1 µM *rac*-GR24. A minimum of 50 seeds were sprinkled on each well, in triplicates. Plates were sealed with Micropore tape and incubated at 33 °C for 7 days in an incubator with continuous light. Germination was scored on day 7 by radicle emergence. Compounds that showed germination reduction as compared with the GR24-only control were carried forward for further analysis.

MD simulations

MD simulations for ShHTL7 in the presence of the RG66-series compounds (complexes obtained by docking as described previously) were performed in triplicate cycles of 0.5 µs using the GROMACS (version 4.5) simulation package (58). The starting coordinates used were those obtained from the ShHTL7–RG6 structure and those obtained by docking. All crystallographic water molecules were removed from the protein file. The substrates (RG66 compounds) were placed in the active site, as described in *Chemical docking* section and validated using the crystallographic structure of ShHTL7–RG6. The force field used was CHARMM36 (59). Amino acids were assumed to be in their standard protonation state at pH 7.0. Hydrogens were added to the .pdb files using the molecule editor Avogadro (60). Ligand topologies were generated using the CGenFF server and validated by the server's penalty score system to ensure that atom types, bond connectivity, and charges were all below a penalty score of 10. The structures were solvated using the pdb2gmx and solvate modules (transferable intermolecular potential with three points water for solvent configuration) and placed in the center of a dodecahedral unit cell (dimensions = 8.49 × 8.49 × 6.33 Å), at least 1 nm from the box edge, filled with simple point–charge water molecules extending to at least 8 Å from the complex atoms. The solvated systems were neutralized by adding Na^+ and Cl^- ions using the genion module.

The systems were initially minimized using 1000 steps steepest descent, followed by conjugate gradient minimization, for a total maximum number of minimization steps of 50,000. To obtain the canonical ensembles (NVT), the minimized systems were heated from 100 to 300 K over 0.04 ns and then for another 0.06 ns for T_m equilibration; T_m was maintained using the Velocity Rescale Thermostat. To obtain isothermal-isobaric ensembles (NPT), the system was equilibrated for 0.1 ns at constant pressure using the modified Berendsen barostat for pressure coupling with isotropic position scaling, with a reference pressure of 1 bar. Continuing from NPT, the equilibrated systems were exposed to a fully unrestrained production simulation of 0.5 µs. All H-bonds were constrained with the linear solver constraint algorithm; long-range electrostatic forces were calculated with particle-mesh Ewald using a time step of 2 fs throughout the simulation.

Finally, the molecules' coordinates were recentered within the unit cell. The number and distance of protein–ligand interactions were calculated using the H-bond module, whereas the rms module was used to quantify the location change of the ligand. Insignificant differences between each simulation replicate were quantified (Table S2); the average RMSD of the ligand after convergence and the average potential energy at the end of each simulation replicate were calculated and recorded (Table S2). Those systems that did not converge for at least one of the simulation replicates were further analyzed but automatically classified as unlikely binders. All simulations were analyzed using the modules mentioned in this section.

The trajectories of the replicates with the lowest potential energy for each simulation were visualized using the Visual MD package (version 1.9.4) using PyMOL (56), the University of California, San Francisco Chimera package, and Final Cut Pro (version 10.5.4 for mac OS BigSur) for graphics production (61). All simulations were carried out in the Cedar compute and Cedar graphics processing unit servers of the Compute Canada Database.

GA-depletion germination

These germination assays were also performed using ShHTL7-expression *Arabidopsis* seeds (*htl-3* background) on 1/2 MS minimal agar medium. Stocks of *rac*-GR24 were prepared in dimethyl sulfoxide, and paclobutrazol was prepared in ethanol. Each stock was diluted 1:1000 in 1/2 MS to a final solvent percentage of 0.1 (v/v). For germination assays, the seeds were at least 1 month old. All seeds were surface sterilized with 70 to 100% (v/v) EtOH. Approximately 50 seeds were used per assay. Several concentrations (0–10 µM) of candidate antagonist were tested in the presence of 1 µM *rac*-GR24 and 15 µM paclobutrazol. After seeds were plated on agar, they were stratified for 4 days at 4 °C and then placed under continuous white light at 25 to 26 °C. After 7 days under continuous white light, germination was scored using radicle emergence.

DSF

DSF experiments were performed on a BioRad CFX96 real-time PCR detection system using the fluorescence resonance energy transfer channel for an excitation (450–490 nm) and emission (560–580 nm) wavelengths. Samples were prepared in triplicate using 5 µg protein and increasing concentrations of ligand (1 µM *rac*-GR24 and 0, 0.5, 1, 2.5, 5, and 10 µM antagonist) in a buffer containing 10 mM Hepes (pH 7.2) and 200 mM NaCl. Following an incubation of 30 min with the

ligand, 0.5 mM SYPRO Orange was added and used as the reporter dye. After an equilibration of 5 min at 5 °C, samples were heat denatured using a linear 5 to 95 °C gradient at a rate of 0.5 °C with intervals of 20 s. Protein unfolding was monitored by detecting changes in SYPRO Orange fluorescence. Melting curves were generated with the GraphPad Prism software (GraphPad Software, Inc), version 9.0.

YLG–GR24 competition assays

In vitro YLG hydrolysis assays were performed using 0.1 μg of purified ShHTL7 in a reaction buffer (20 mM Hepes, 150 mM NaCl, pH 7.0) at a 100 μl volume on a 96-well black plate (Greiner). The protein was mixed with increasing concentrations (0, 0.1, 0.15, 0.2, 0.3, 0.5, 1, 2.5, 5, 10, 15, and 20 μM) of antagonist or *rac*-GR24 and kept on ice. The fluorescence intensity was immediately measured using a TECAN machine with an excitation wavelength of 480 nm and a detection wavelength of 520 nm. Fluorescence values reported were obtained by subtracting the fluorescence signal obtained from YLG + antagonist-only controls. IC_{50} values were calculated by fitting competition assay values in a sigmoid curve using the GraphPad Prism software, version 9.0.

Striga *germination and conditioning-DOZ exposure assays*

S. hermonthica seeds were surface sterilized in a 0.7% bleach/double-distilled water (v/v) solution two times and then washed several times with sterile MilliQ deionized water to remove excess bleach.

At least 50 seeds were used for all experiments described in this section. Seeds were water-imbibed on a filter paper and conditioned at 30 °C in the dark. After 14 days, seeds were gently washed three times from the filter paper using sterile MilliQ deionized water and plated on 48-well plates containing 1 μM *rac*-GR24 and increasing concentrations (0–20 μM) of antagonist in 100 μl volumes. Seeds were incubated under white light for 2 days, and germination was scored by radicle emergence. Germination scores were plotted, and EC_{50} values were calculated using three biological replicates.

For the DOZ-SL conditioning experiments, seeds were water-imbibed or 0.1 μM DOZ-imbibed on a filter paper and conditioned at 30 °C in the dark. After 14 days, seeds were gently washed three times from the filter paper using sterile MilliQ deionized water to remove any excess chemical and plated on 48-well plates containing 100 μl 0.1 or 1 μM *rac*-GR24. Seeds were incubated under white light for 2 days, and germination was scored by radicle emergence. Germination scores were plotted using three biological replicates.

For the DOZ-time exposure experiments, seeds were water-imbibed on a filter paper and conditioned at 30 °C in the dark. After 14 days, seeds were gently washed three times from the filter paper using sterile MilliQ deionized water. Then, seeds were incubated in the dark at 30 °C in the presence of 0.1 μM *rac*-GR24 and 1 μM DOZ for different periods between 0 and 24 h. After a set amount of time, a batch of seeds would be removed and gently washed three times using sterile MilliQ deionized water. Finally, seeds were placed on 48-well plates containing 100 μl 0.1 μM *rac*-GR24 and incubated under white light for 1 day after which germination was scored by radicle emergence. Germination scores were plotted using three biological replicates. All graphs in this section were prepared using the GraphPad Prism software, version 9.0.

Data availability

All data described in this study are contained within the article; any additional data will be shared upon request to Peter McCourt, peter.mccourt@utoronto.ca.

Supporting information—This article contains supporting information.

Acknowledgments—This research was enabled in part by support provided by Compute Ontario (https://computeontario.ca/) and Compute Canada (www.computecanada.ca). We express our gratitude for technical advice provided by R. DiLeo, T. Skarina, E. Edvokimova, V. Yim, Dr Y. Tsuchiya, Dr M. Venkatesan, C. Pham, Dr Z. Xu, and Dr J. Bradley.

Author contributions—A. A.-S., A. S., and S. L. investigation; P. J. S., C. S., and P. M. methodology; A. A.-S. and P. M. writing–original draft; and S. L. and P. J. S. writing–review and editing.

Funding and additional information—A. A.-S. was partially funded by the Mexican National Council of Science and Technology (CONACyT) and by a Mitacs Globalink Graduate Scholarship. This work was supported by a Natural Sciences and Engineering Research Council of Canada (NSERC) Discovery grant (grant no.: 06752), an NSERC Accelerator Supplement (grant no.: 507992), an NSERC Research Tools and Instruments grant (grant no.: 00356), a New Frontiers in Research Fund (grant no.: NFRFE-2018-00118) awarded to S. L., as well as an NSERC Discovery grant (grant no.: 04298) awarded to P. M.

Conflict of interest—The authors declare that they have no conflicts of interest with the contents of this article.

Abbreviations—The abbreviations used are: DOZ, dormirazine; DSF, differential scanning fluorimetry; GA, gibberellin; MD, molecular dynamics; MS, Murashige and Skoog; NPT, isothermal-isobaric ensembles; NSERC, Natural Sciences and Engineering Research Council of Canada; NVT, canonical ensembles; PDB, Protein Data Bank; ShHTL, *Striga hermonthica* HYPOSENSITIVE TO LIGHT; SL, strigolactone; SPL7, sphynolactone-7; YLG, Yoshimulactone Green.

References

1. Fernández-Aparicio, M., Delavault, P., and Timko, M. P. (2020) Management of infection by parasitic weeds: A review. *Plants* **9**, 1184
2. Parker, C. (2009) Observations on the current status of *Orobanche* and *Striga* problems worldwide. *Pest Manag. Sci.* **65**, 453–459
3. Scholes, J. D., and Press, M. C. (2008) Striga infestation of cereal crops - an unsolved problem in resource limited agriculture. *Curr. Opin. Plant Biol.* **11**, 180–186

4. Hearne, S. J. (2009) Control–the *Striga* conundrum. *Pest Manag. Sci.* **65**, 603–614
5. Tippe, D. E., Rodenburg, J., Schut, M., van Ast, A., Kayeke, J., and Bastiaans, L. (2017) Farmers' knowledge, use and preferences of parasitic weed management strategies in rain-fed rice production systems. *Crop Prot.* **99**, 93–107
6. Hu, L., Wang, J., Yang, C., Islam, F., Bouwmeester, H. J., Muños, S., and Zhou, W. (2020) The effect of virulence and resistance mechanisms on the interactions between parasitic plants and their hosts. *Int. J. Mol. Sci.* **21**, 9013
7. Samejima, H., Babiker, A. G., Takikawa, H., Sasaki, M., and Sugimoto, Y. (2016) Practicality of the suicidal germination approach for controlling *Striga hermonthica*. *Pest Manag. Sci.* **72**, 2035–2042
8. Xie, X., Yoneyama, K., and Yoneyama, K. (2010) The strigolactone story. *Annu. Rev. Phytopathol.* **48**, 93–117
9. Gobena, D., Shimels, M., Rich, P. J., Ruyter-spira, C., Bouwmeester, H., and Kanuganti, S. (2017) Mutation in sorghum *LOW GERMINATION STIMULANT 1* alters strigolactones and causes *Striga* resistance. *Proc. Natl. Acad. Sci. U. S. A.* **114**, 4471–4476
10. Mohemed, N., Charnikhova, T., Bakker, E. J., van Ast, A., Babiker, A. G., and Bouwmeester, H. J. (2016) Evaluation of field resistance to *Striga hermonthica* (Del.) Benth. in Sorghum bicolor (L.) Moench. The relationship with strigolactones. *Pest Manag. Sci.* **72**, 2082–2090
11. Uraguchi, D., Kuwata, K., Hijikata, Y., Yamaguchi, R., Imaizumi, H., Am, S., Rakers, C., Mori, N., Akiyama, K., Irle, S., McCourt, P., Kinoshita, T., Ooi, T., and Tsuchiya, Y. (2018) A femtomolar-range suicide germination stimulant for the parasitic plant *Striga hermonthica*. *Science* **362**, 1301–1305
12. Zwanenburg, B., Mwakaboko, A. S., and Kannan, C. (2016) Suicidal germination for parasitic weed control. *Pest Manag. Sci.* **72**, 2016–2025
13. Lumba, S., Subha, A., and McCourt, P. (2017) Found in translation: Applying lessons from model systems to strigolactone signaling in parasitic plants. *Trends Biochem. Sci.* **42**, 556–565
14. Matusova, R., van Mourik, T., and Bouwmeester, H. J. (2004) Changes in the sensitivity of parasitic weed seeds to germination stimulants. *Seed Sci. Res.* **14**, 335–344
15. Tsuchiya, Y., Yoshimura, M., Sato, Y., Kuwata, K., Toh, S., Holbrook-Smith, D., Zhang, H., McCourt, P., Itami, K., Kinoshita, T., and Hagihara, S. (2015) PARASITIC PLANTS. Probing strigolactone receptors in *Striga hermonthica* with fluorescence. *Science* **349**, 864–868
16. Toh, S., Holbrook-Smith, D., Stogios, P. J., Onopriyenko, O., Lumba, S., Tsuchiya, Y., Savchenko, A., and McCourt, P. (2015) Structure-function analysis identifies highly sensitive strigolactone receptors in Striga. *Science* **350**, 203–207
17. Mashiguchi, K., Seto, Y., and Yamaguchi, S. (2021) Strigolactone biosynthesis, transport and perception. *Plant J.* **105**, 335–350
18. Flematti, G. R., Scaffidi, A., Waters, M. T., and Smith, S. M. (2016) Stereospecificity in strigolactone biosynthesis and perception. *Planta* **243**, 1361–1373
19. Miyakawa, T., Xu, Y., and Tanokura, M. (2020) Molecular basis of strigolactone perception in root-parasitic plants: Aiming to control its germination with strigolactone agonists/antagonists. *Cell. Mol. Life Sci.* **77**, 1103–1113
20. Takeuchi, J., Jiang, K., Hirabayashi, K., Imamura, Y., Wu, Y., Xu, Y., Miyakawa, T., Nakamura, H., Tanokura, M., and Asami, T. (2018) Rationally designed strigolactone analogs as antagonists of the D14 receptor. *Plant Cell Physiol.* **59**, 1545–1554
21. Nakamura, H., Hirabayashi, K., Miyakawa, T., Kikuzato, K., Hu, W., Xu, Y., Jiang, K., Takahashi, I., Niiyama, R., Dohmae, N., Tanokura, M., and Asami, T. (2019) Triazole ureas covalently bind to strigolactone receptor and antagonize strigolactone responses. *Mol. Plant* **12**, 44–58
22. Shahul Hameed, U., Haider, I., Jamil, M., Kountche, B. A., Guo, X., Zarban, R. A., Kim, D., Al-Babili, S., and Arold, S. T. (2018) Structural basis for specific inhibition of the highly sensitive ShHTL7 receptor. *EMBO Rep.* **19**, e45619
23. Holbrook-Smith, D., Toh, S., Tsuchiya, Y., and McCourt, P. (2016) Small-molecule antagonists of germination of the parasitic plant *Striga hermonthica*. *Nat. Chem. Biol.* **12**, 724–729
24. Hamiaux, C., Drummond, R. S., Janssen, B. J., Ledger, S. E., Cooney, J. M., Newcomb, R. D., and Snowden, K. C. (2012) DAD2 is an α/β hydrolase likely to be involved in the perception of the plant branching hormone, strigolactone. *Curr. Biol.* **22**, 2032–2036
25. Zhao, L.-H., Zhou, X. E., Wu, Z.-S., Yi, W., Xu, Y., Li, S., Xu, T. H., Liu, Y., Chen, R. Z., Kovach, A., Kang, Y., Hou, L., He, Y., Xie, C., Song, W., *et al.* (2013) Crystal structures of two phytohormone signal-transducing α/β hydrolases: Karrikin-signaling KAI2 and strigolactone-signaling DWARF14. *Cell Res.* **23**, 436–439
26. Xu, Y., Miyakawa, T., Nosaki, S., Nakamura, A., Lyu, Y., Nakamura, H., Ohto, U., Ishida, H., Shimizu, T., Asami, T., and Tanokura, M. (2018) Structural analysis of HTL and D14 proteins reveals the basis for ligand selectivity in *Striga*. *Nat. Commun.* **9**, 3947
27. Yao, R., Ming, Z., Yan, L., Li, S., Wang, F., Ma, S., Yu, C., Yang, M., Chen, L., Chen, L., Li, Y., Yan, C., Miao, D., Sun, Z., Yan, J., *et al.* (2016) DWARF14 is a non-canonical hormone receptor for strigolactone. *Nature* **536**, 469–473
28. Arellano-Saab, A., Bunsick, M., Al Galib, H., Zhao, W., Schuetz, S., Bradley, J. M., Xu, Z., Adityani, C., Subha, A., McKay, H., de Saint Germain, A., Boyer, F. D., McErlean, C. S. P., Toh, S., McCourt, P., *et al.* (2021) Three mutations repurpose a plant karrikin receptor to a strigolactone receptor. *Proc. Natl. Acad. Sci. U. S. A.* **118**, e2103175118
29. Bürger, M., Mashiguchi, K., Lee, H. J., Nakano, M., Takemoto, K., Seto, Y., Yamaguchi, S., and Chory, J. (2019) Structural basis of karrikin and non-natural strigolactone perception in *Physcomitrella patens*. *Cell Rep.* **26**, 855–865
30. Wang, Y., Yao, R., Du, X., Guo, L., Chen, L., Xie, D., and Smith, S. M. (2021) Molecular basis for high ligand sensitivity and selectivity of strigolactone receptors in *Striga*. *Plant Physiol.* **185**, 1411–1428
31. Morris, G., Huey, R., Lindstrom, W., Sanner, M., Belew, R., Goodsell, R., and Olson, A. (2009) AutoDock4 and AutoDockTools4: Automated docking with selective receptor flexibility. *J. Comput. Chem.* **16**, 2785–2791
32. Grosdidier, A., Zoete, V., and Michielin, O. (2011) SwissDock, a protein-small molecule docking web service based on EADock DSS. *Nucleic Acids Res.* **39**, 270–277
33. Toh, S., Kamiya, Y., Kawakami, N., Nambara, E., McCourt, P., and Tsuchiya, Y. (2012) Thermoinhibition uncovers a role for strigolactones in Arabidopsis seed germination. *Plant Cell Physiol.* **53**, 107
34. Bunsick, M., Toh, S., Wong, C., Xu, Z., Ly, G., McErlean, C. S. P., Pescetto, G., Nemrish, K. E., Sung, P., Li, J. D., Scholes, J. D., and Lumba, S. (2020) SMAX1-dependent seed germination bypasses GA signalling in Arabidopsis and Striga. *Nat. Plants* **6**, 646–652
35. Lee, H. W., Sharma, P., Janssen, B. J., Drummond, R. S. M., Luo, Z., Hamiaux, C., Collier, T., Allison, J. R., and Newcomb, R. D. (2020) Flexibility of the petunia strigolactone receptor DAD2 promotes its interaction with signaling partners. *J. Biol. Chem.* **295**, 4181–4193
36. Bai, N., Roder, H., Dickson, A., and Karanicolas, J. (2019) Isothermal analysis of thermofluor data can readily provide quantitative binding affinities. *Sci. Rep.* **9**, 2650
37. Dubach, J. M., Kim, E., Yang, K., Cuccarese, M., Giedt, R. J., Meimetis, L. G., Vinegoni, C., and Weissleder, R. (2017) Quantitating drug-target engagement in single cells in vitro and in vivo. *Nat. Chem. Biol.* **13**, 168–173
38. García-Contreras, R., Vos, P., Westerhoff, H. V., and Boogerd, F. C. (2007) Why *in vivo* may not equal *in vitro* - new effectors revealed by measurement of enzymatic activities under the same *in vivo* -like assay conditions. *FEBS J.* **279**, 4145–4159
39. McEneny-King, A., Edginton, A. N., and Rao, P. P. N. (2015) Investigating the binding interactions of the anti-Alzheimer's drug donepezil with CYP3A4 and P-glycoprotein. *Bioorg. Med. Chem. Lett.* **25**, 297–301
40. Baskin, J., and Baskin, C. (2004) A classification system for seed dormancy. *Seed Sci. Res.* **14**, 1–16
41. Takahashi, I., and Asami, T. (2018) Target-based selectivity of strigolactone agonists and antagonists in plants and their potential use in agriculture. *J. Exp. Bot.* **69**, 2241–2254

42. Moffat, J. G., Vincent, F., Lee, J. A., Eder, J., and Prunotto, M. (2017) Opportunities and challenges in phenotypic drug discovery: An industry perspective. *Nat. Rev. Drug Discov.* **16**, 531–543
43. Hamiaux, C., Drummond, R. S. M., Luo, Z., Lee, H. W., Sharma, P., Janssen, B. J., Perry, N. B., Denny, W. A., and Snowden, K. C. (2018) Inhibition of strigolactone receptors by *N*-phenylanthranilic acid derivatives: Structural and functional insights. *J. Biol. Chem.* **293**, 6530–6543
44. Bürger, M., and Chory, J. (2020) In-silico analysis of the strigolactone ligand-receptor system. *Plant Direct* **4**, e00263
45. De Vivo, M., Masetti, M., Bottegoni, G., and Cavalli, A. (2016) Role of molecular dynamics and related methods in drug discovery. *J. Med. Chem.* **59**, 4035–4061
46. Pinzi, L., and Rastelli, G. (2019) Molecular docking shifting paradigms in drug discovery. *Int. J. Mol. Sci.* **18**, 4331
47. Jumper, J., Evans, R., Pritzel, A., Green, T., Figurnov, M., Ronneberger, O., Tunyasuvunakool, K., Bates, R., Žídek, A., Potapenko, A., Bridgland, A., Meyer, C., Kohl, S. A. A., Ballard, A. J., Cowie, A., *et al.* (2021) Highly accurate protein structure prediction with AlphaFold. *Nature* **596**, 583–589
48. Baek, M., DiMaio, F., Anishchenko, I., Dauparas, J., Ovchinnikov, S., Lee, G. R., Wang, J., Cong, Q., Kinch, L. N., Schaeffer, R. D., Millán, C., Park, H., Adams, C., Glassman, C. R., DeGiovanni, A., *et al.* (2021) Accurate prediction of protein structures and interactions using a three-track neural network. *Science* **373**, 871–876
49. Gurney, A. L., Press, M. C., and Scholes, J. D. (1999) Infection time and density influence the response of sorghum to the parasitic angiosperm *Striga hermonthica*. *New Phytol.* **143**, 573–580
50. Tippe, D. E., Rodenburg, J., and van Ast, A. (2017) Delayed or early sowing: Timing as parasitic weed control strategy in rice is species and ecosystem dependent. *Field Crops Res.* **214**, C14–C24
51. Yoneyama, K., Awad, A., Xie, X., Yoneyama, K., and Takeuchi, Y. (2010) Strigolactones as germination stimulants for root parasitic plants. *Plant Cell Physiol.* **51**, 1095–1103
52. Skarina, T., Xu, X., Evdokimova, E., and Savchenko, A. (2014) High throughput crystallization screening. *Methods Mol. Biol.* **1140**, 159–168
53. Minor, W., Cymborowski, M., Otwinowski, Z., and Chruszcz, M. (2006) HKL-3000: The integration of data reduction and structure solution—from diffraction images to an initial model in minutes. *Acta Crystallogr. D Biol. Crystallogr.* **62**, 859–866
54. Adams, P. D., Afonine, P. V., Bunkóczi, G., Chen, V. B., Davis, I. W., Echols, N., Headd, J. J., Hung, L. W., Kapral, G. J., Grosse-Kunstleve, R. W., McCoy, A. J., Moriarty, N. W., Oeffner, R., Read, R. J., Richardson, D. C., *et al.* (2010) PHENIX: A comprehensive Python-based system for macromolecular structure solution. *Acta Crystallogr. D Biol. Crystallogr.* **66**, 213–221
55. Emsley, P., and Cowtan, K. (2004) Coot: Model-building tools for molecular graphics. *Acta Crystallogr. D Biol. Crystallogr.* **60**, 2126–2132
56. Schrödinger (2015) *The PyMOL Molecular Graphics System, Version 2.0.* Schrödinger, LLC
57. Laskowski, R., and Swindells, M. (2011) LigPlot+: Multiple ligand-protein interaction diagrams for drug discovery. *J. Chem. Inf. Model.* **51**, 2778–2786
58. Abraham, M. J., Murtola, T., Schulz, R., Páll, S., Smith, J., Hess, B., and Lindahl, E. (2015) GROMACS: High performance molecular simulations through multi-level parallelism from laptops to supercomputers. *SoftwareX* **1–2**, 19–25
59. Huang, J., Rauscher, S., Nawrocki, G., Ran, T., Feig, M., de Groot, B., Grubmüller, H., and MacKerell, D., Jr. (2017) CHARMM36m: An improved force field for folded and intrinsically disordered proteins. *Nat. Methods* **14**, 71–73
60. Hanwell, M. D., Curtis, D., Lonie, D., Vandermeersch, T., Zurek, E., and Hutchison, G. E. (2012) Avogadro: An advanced semantic chemical editor, visualization, and analysis platform. *J. Cheminform.* **4**, 17
61. Humphrey, W., Dalke, A., and Schulten, K. (1996) VMD: Visual molecular dynamics. *J. Mol. Graph.* **14**, 33–38